RSC Advances

PAPER

View Article Online
View Journal | View Issue

Cite this: *RSC Adv.*, 2022, **12**, 9292

Analysis of gold nanospheres, nano ellipsoids, nanorods, and effect of core–shell structures for hyperthermia treatment

Ghulam Abbas,[a] Saba Maqbool,[a] Muhammad Khuram Shahzad, *[b] Muhammad Afzaal,[a] Muhammad Usama Daud,[a] Nazma Goher Fatima[a] and Abdul Ghuffar[a]

Received 29th January 2022
Accepted 5th March 2022

DOI: 10.1039/d2ra00618a

rsc.li/rsc-advances

Hyperthermia (HT) is a technique for treating malignancies by raising the temperature of the defected tissues. This technique has been used as a treatment to raise tumor area temperatures between 42 °C to 48 °C. Hyperthermia penetrates deeper malignant cells by heating the region of interest when magnetic nanoparticles (MNPs) are exposed to an externally induced magnetic field of the incident wave. In this work, numerical analysis was used to examine the temporal and spatial temperature distributions within a tumor. The temperature field was analyzed using the mass transfer and diffusion theories in the interstitial tissue. A bio-heating module in COMSOL Multi-Physics was used for different types of gold nanoparticles (AuNPs) including nanorods, nanospheres, and nano-ellipsoids with different shapes. The objective of this study is to analyze the use of AuNPs for hyperthermia. The results show that AuNPs achieve a maximum temperature for Au nanorods as compared to nano ellipsoids and nanospheres. The Au NPs achieve thermal equilibrium after 0.5 μs and are effective for hyperthermia treatment. The results describe the effect of nanoparticle shape and surface coating on thermal absorption around the nanoparticle in hyperthermia. The significance of Au NPs for hyperthermia is explained. It is expected that this study will be helpful in the future for hyperthermia treatment.

1. Introduction

Cancer is a disease in which a cell group grows uncontrollably. Cancerous cells do not answer the signals that stimulate the regular cell cycle as their self-sufficiency is unregulated, resulting in uncontrolled cell growth and proliferation.[1] Hyperthermia therapies are commonly used in combination with other cancer treatments such as chemotherapy or radiation therapy because heat-stressed cells are more responsive to treatment.[2,3] This method of treatment uses external physical methods to increase the temperature of the tumor region between 42 °C to 48 °C. An increase in temperature can be localized or systemic, affecting the entire body and its treatment strategy. Hyperthermia consists of three types, local hyperthermia, regional hyperthermia, and whole-body hyperthermia. Local hyperthermia (LHT) has fewer side effects as compared to chemo- and radiation, and it may be used in conjunction with all conventional treatment techniques.[4] There are three main clinical methods of high-temperature applications, regulated by the organ to target the tumor's stage. Localized, progressing or deep-seated, and disseminated cancers get heat through localized, regional, and whole-body HT, respectively. Local HT is reserved for small tumors (≤3 cm to 5–6 cm in diameter) located superficially or within an accessible bodily cavity, including the rectum or esophagus.[5] To deliver heat to tumors, superficial, intraluminal applicators are used in local HT. And microwaves, radio waves, or ultrasound is mostly used.[6] It is typically used to treat advanced cancers of the pelvis, abdomen, or thighs.[7] There are three most important approaches: intrinsic (tumors heated with peripheral applicators), thermal (organs or limbs treated with thermal perfusion), and continuous hyperthermic peritoneal perfusion (CHPP).[8] The usage of radiation heat or extracorporeal technology to raise the temperature of the entire body to at least 41 °C is known as whole-body hyperthermia (WBH).[9–12]

Gold and its alloys have been utilized in medicine since its discovery over 5000 years ago.[13] Metallic nanoparticles, such as gold (Au), exhibit unique electrical and optical properties, as well as chemical inertness and the capacity to surface functionalize, due to the positive potential on their surface.[14] These electrical and optical properties have ensured its use in biosensors, bio-imaging, and photo-thermal treatment.[15] Gold (Au) can be conjugated with ligands, antibodies, or pharmacological molecules for active or passive medication due to its enhanced functionalization with organic molecules.[16] Because

[a]Department of Physics, Riphah International University Faisalabad Campus, Pakistan
[b]Department of Physics, Khawaja Fareed University of Engineering & Information Technology, Rahim Yar Khan, Pakistan. E-mail: khuram.shahzad@kfueit.edu.pk; muhammad.afzaal@riphahfsd.edu.pk

of gold's chemical inertness, it has high biocompatibility both *in vitro* and *in vivo*.[17–19] While nanoparticles of 20–60 nm appear to have the greatest cellular absorption, they also cause systemic toxicity due to liver, lung, and spleen damage, as opposed to smaller 5–10 nm.[20–23] When considering the mass of Au NP, the optimal size expressed as the number of particles in a cell may vary, referring to the complexity of Au NP size and its influence on bioavailability and cellular absorption.[24–26] Au is used to

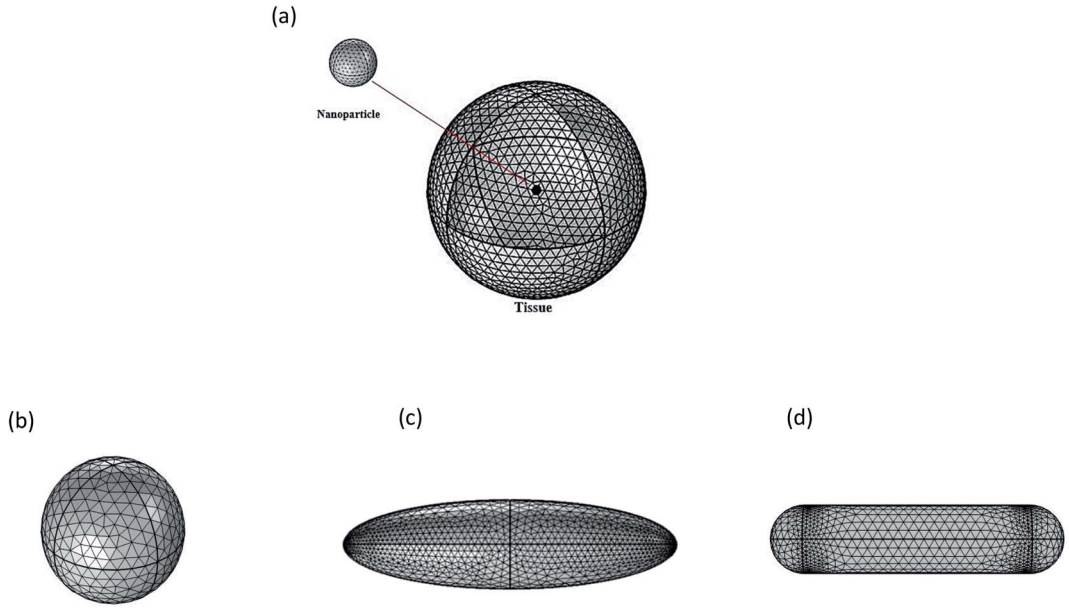

Fig. 1 (a) Nanoparticle placed within a spherical tissue (b) nanosphere, (c) nano ellipsoid, (d) nanorod.

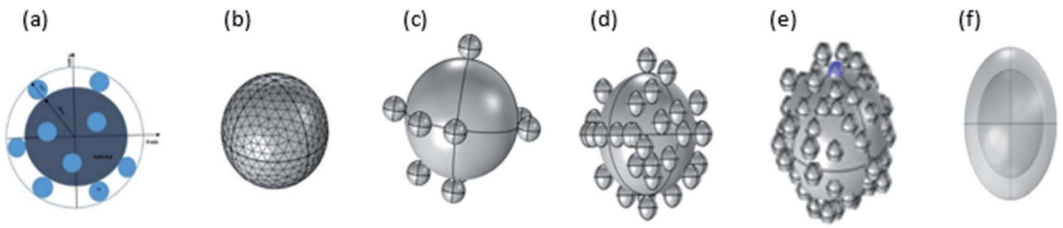

Fig. 2 COMSOL simulation of an incomplete shell structure (a) bare core with the radius 20 nm, AgNPs of 4 nm radius attached to core surface (b) core (c) 10 NPs, (d) 40 NPs (e) 70 NPs attached to the core (f) complete shell.

Table 1 Different studies for comparison

Study type and year	Particle type and size	Coating	Results and drawbacks	References
Animal clinical studies (photo thermal hyperthermia) (2015)	(5–8 nm) of lipos Au NPs	Gold coated	For treatment of specific tumors biodegradable NPs system is suitable	32
Test tube experiment (magnetic hyperthermia) (2008)	10 nm of polymer encapsulated Fe_2O_3	—	Non-uniform size loading to heating profiles It was suitable for evaluating magnetic nano fluid transport	33
Magnetic hyperthermia (2010)	1–100 nm of silica–Fe_2O_3	—	There is the direct real- time lacking of visual control of magnetic fluid injection It was suitable for thermal ablation of prostate cancer	34
Magnetic hyperthermia (2009)	19 nm radius of magnetite and 9 nm of iron platinum	—	Reaches steady state after 300 s	35

treating diseases such as smallpox, skin ulcers, and measles.[27–31]

Lin C. and Liu K.[35] studied theoretically the hyperthermia effect and concluded that the particles reach steady state after 300 s and it is very large time to reach steady state. Keeping the mind the properties of gold nanoparticles (AuNPs) our main concern was to measure the less time to reach steady state. In this work, we study the heat generation of a single nanoparticle (Au) of different shapes (sphere, cube, and rod) and volume ($V_{sphere} = V_{cube} = V_{rod}$) placed in a spherical cell or tissue area. The proposed model reflects the spatial-temporal temperature distribution as well as the thermal effects generated by heat propagation in the tumor cell. Based on the thermal properties of chosen materials, we study the effect of different coating materials, like polymer and gold, on the system's temperature response (augmentation/diminution). An incomplete coating surface with varying amounts of nanoparticles connected to the surface of the magnetic core, as well as the associated hyperthermia behavior, were simulated. COMSOL Multiphysics (heat transfer module) was used to perform finite element simulations of the heating process of nanoparticles. The simulations explore the temperature distribution within the nanoparticle (heat dissipation).[32–34]

2. Material and methods

In this work, a single nanoparticle inside 0.5 μm radius with the spherical domain of tissue was considered for different shapes and used in this simulation are given in Fig. 1.

The fundamental goal was to explore the temperature behavior of biological tissue when a nanoparticle is exploited as a heating source having a complex core–shell structure and having various shapes (sphere, ellipsoid, and rod).

The temperature distribution T (x, y, z, and t) in the tumor cell is given by the solution of the Fourier heat transport equation:

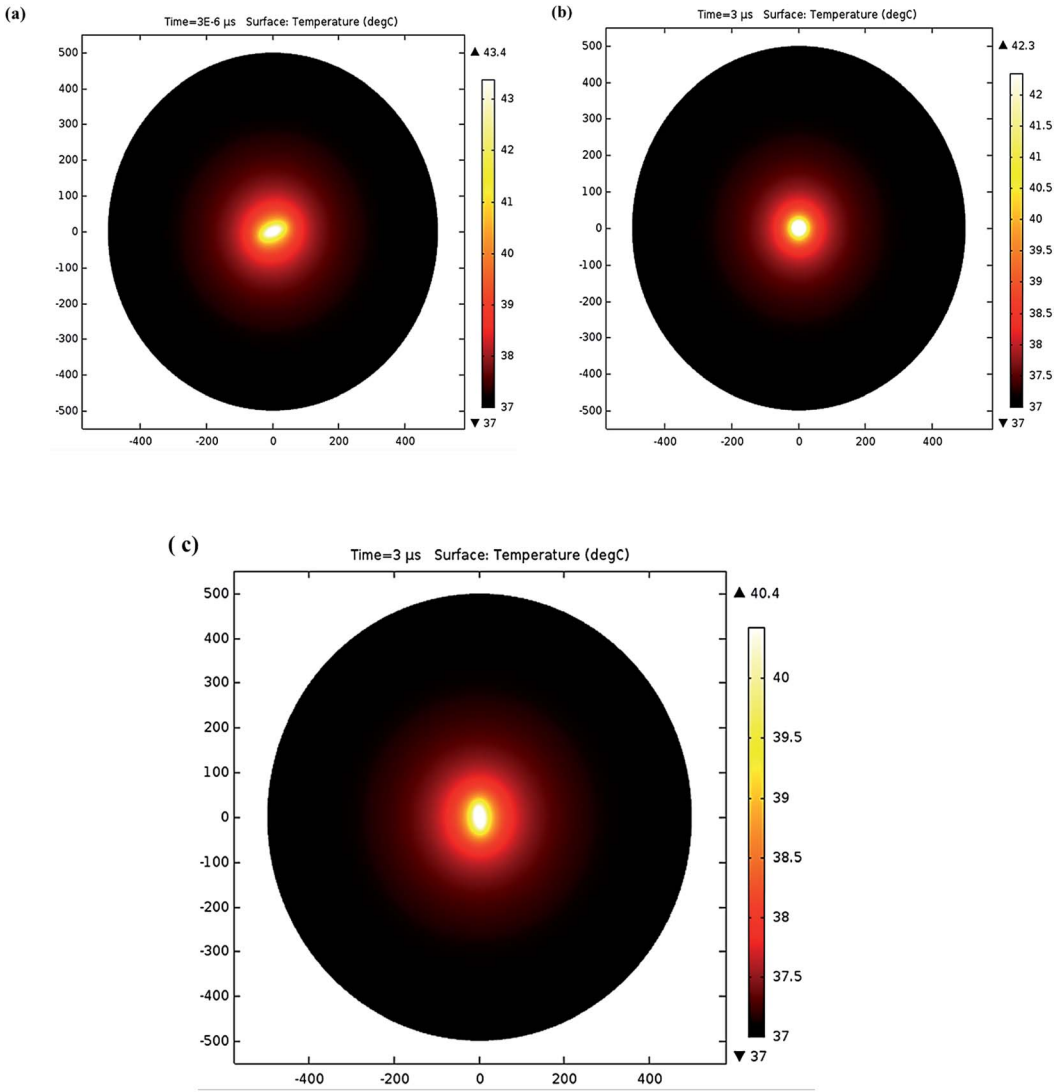

Fig. 3 The 2D spatial temperature distribution of 0.5 μm tumoral cell from the start of the heating process for, nano-rod (11, 73, 11) nm nano-sphere (20 nm), and nano-ellipsoid (12, 15, 44.3) nm.

$$\rho C_p \frac{\partial T}{\partial t} + \nabla(-k\nabla T) = Q \quad (1)$$

where ρ is the cell density, C_p is the specific heat capacity at constant pressure, k is the thermal conductivity of the cell, and the heat dissipated by nanoparticles in the cell volume is denoted by Q. The volumetric power density is constant, and its value is $Q = 10^{16}$ (W m^{-3}). To study the heating process, the initial temperature of the tissue was kept $T_i = 37$ °C, which is the normal temperature of the human body. Magnetic nanoparticles (MNP) and tissue geometry are discretized on all domains with free tetrahedral components, providing a full mesh of 58 272 domain elements.

The following are the specifications that are considered:

(1) The tumor cell totally absorbs the particle's heat flux (the continuity of the thermal flux between domains).

(2) The temperature of the tissue's outer surface is maintained at $T_0 = 37$ °C, which is human body normal temperature.

A spherical gold NP of radius $r = 20$ nm was considered to study the temporal distribution inside the tissue. The dimensions of the gold nano ellipsoid and gold nanorod were calculated to obtain the same volume for nanosphere, nano ellipsoid and nanorod. A nano-ellipsoid particle with side length of $L_{cyl} = 32$ nm, while a nanorod with a cylindrical shape with length of $L_{cyl} = 73$ nm and hemispherical caps with a radius of $R_{cyl} = R_{cap} = 11$ nm were considered.

Two different types of materials (Ag and PEG polymer) were used to construct the nano shell to study the impact of coating surface thickness (5, 10, 20 and 40 nm). For thermal evolution of nanostructure, core–shell with radius 20 nm was selected. To compare the thermal response of spherical and ellipsoidal surface coating, three distinct coating surfaces (one spherical and two ellipsoidal) were simulated on gold nanoparticles core. Fig. 2 shows the simulation growth of silver nanoparticle on gold core–shell. Table 1 shows the

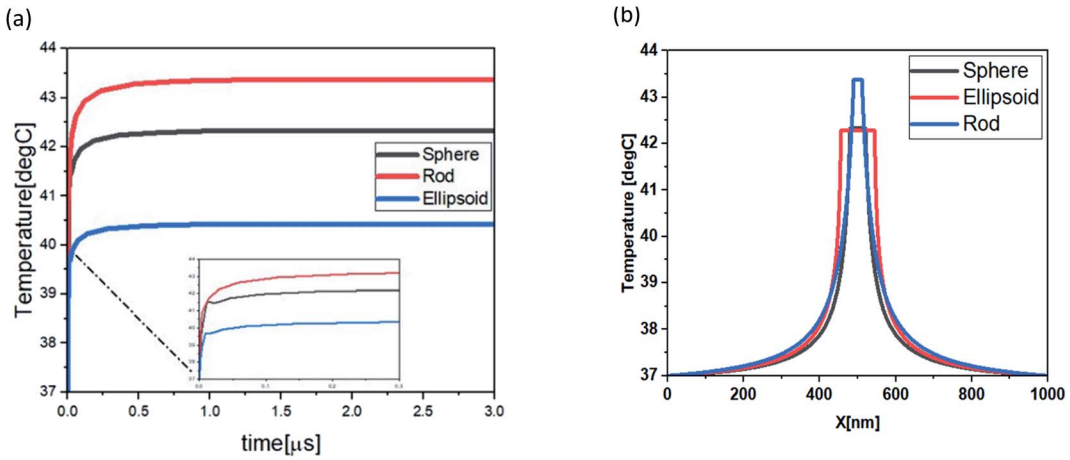

Fig. 4 The temperature's temporal and radial evolution for the three various NPs shapes (nano-sphere, nano-ellipsoid and nano-rod). (a) The temporal evolution at $x = 0$ (center of the heat source). (b) The radial temperature distribution for 3 μs after the heating process began.

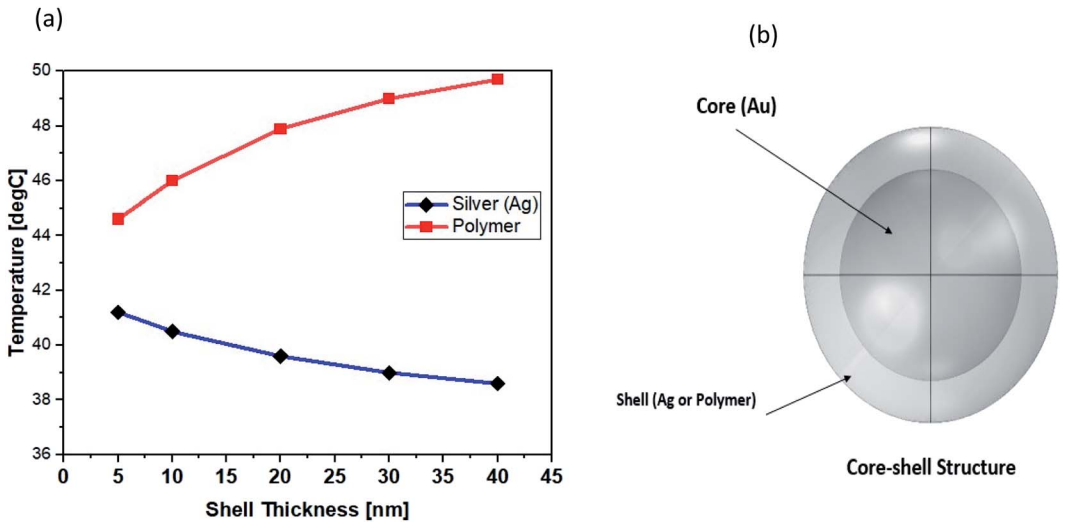

Fig. 5 (a) Surface coating thicknesses (5, 10, 20, 30, and 40 nm) were used to achieve the maximum temperature: silver (blue line) and polymer (red line). (b) The structure of gold core–shell.

thermal properties of different materials that are used in simulation.

3. Results and discussion

To study the potential use of gold nanoparticles (Au NPs) in hyperthermia, gold NPs were inserted radius 500 nm of various shapes such as nano-rod, nano-sphere and, nano-ellipsoid. Fig. 3 shows that the maximum temperature for Au nanorod, Au nanosphere and Au nano ellipsoid was 43.4 °C, 42.3 °C and 40.4 °C respectively. The time evolution of temperature and thermal stability of the tumor tissues cell was measured by heating nanoparticle, as shown in Fig. 3. The temperature difference was achieved by the simulated shapes, this temperature difference can be explained by the proportional surface difference of each shape, given that the thermal response is dependent on heat generation by unit of volume (general heat source) and unit of surface (boundary heat source), as shown in Fig. 4(a). The maximum temperature values are $T_{\max\ \mathrm{rod}} = 43.4\ ^{\circ}\mathrm{C}$ $T_{\max\ \mathrm{sphere}} = 42.3\ ^{\circ}\mathrm{C}$, and $T_{\min\ \mathrm{ellipsoid}} = 40.4\ ^{\circ}\mathrm{C}$. These maximum temperatures are achieved at the center of the particles and spread across the surrounding medium. The distribution of the thermal field in the therapeutic range achieved by rod shape is larger than sphere and ellipsoid as shown in Fig. 4(b).

To explore a functional NP (core–shell structure) in the hyperthermia process, a spherical geometry radius of 20 nm was selected to achieve the maximum temperature for the defined nanoparticle volume. The core of AuNPs was covered by a shell of silver (Ag) or PEG polymer, and the induced temperature by the core was examined. Fig. 5 depicts the variation in heat transfer for various shell thicknesses. Fig. 5(a) shows that as there is increase in silver shell structure results gradually decrease in temperature. For PEG polymer shell, when shell thickness increases then temperature also increases. Silver shell has a greater value of conductivity, as compared to PEG. It transfers quickly the heat generated by core–shell structure to the external medium. To achieve the temperature for hyperthermia, selection of the suitable material and shell thickness depends upon the specific region of the human body (Table 2).[40]

Functionality of NPs can be improved by different shapes of irregular coating. For this purpose, different shapes sphere, $\mathrm{ellipsoid}_1$ and $\mathrm{ellipsoid}_2$ were simulated as shown Fig. 6. The temperature distribution for three different types of surface coating (Fig. 6), a spherical shell 30 nm in radius and two ellipsoids ($\mathrm{ellipsoid}_1$: 25-25-43.2 nm, $\mathrm{ellipsoid}_2$: 22-25-49 nm) with $V_{\mathrm{sphere}} = V_{\mathrm{elipsoid}_1} = V_{\mathrm{elipsoid}_2}$ were compared to investigate the irregular coating surface.

There is very minute difference in temperature *i.e.*, 43.4 °C, 43.2 °C and 43.1 °C which shows that there is no importance of coating surfaces anisotropy for hyperthermia process. Due to the unique properties of silver nanoparticles (AgNPs), they grow and form isolated islands on incomplete irregular coatings, which then transform into a complete shell covering the core. Small AgNPs with a radius of 4 nm were attached to the core surface of 20 nm Ag NPs, which were then embedded in tissue with a radius of 0.5 μm. To define a temperature profile for an incompletely covered NP with a variable number of attached NPs.[41,42]

As shown in Fig. 7, the volume-coverage ratio (percent) of AuNPs in relation to the volume of the entire shell was

Table 2 Thermal properties of the different materials

Thermal conductivity [W m^{-1} K^{-1}]	Mass density [kg m^{-3}]	Specific heat capacity [J kg^{-1} K^{-1}]	References
0.512	1000	3800	Tissue[35]
71	21 500	132	Tumor[36]
317	19 300	129	Gold[37]
429	10 500	235	Silver[38]
0.2	1000	1000	Polymer[39]

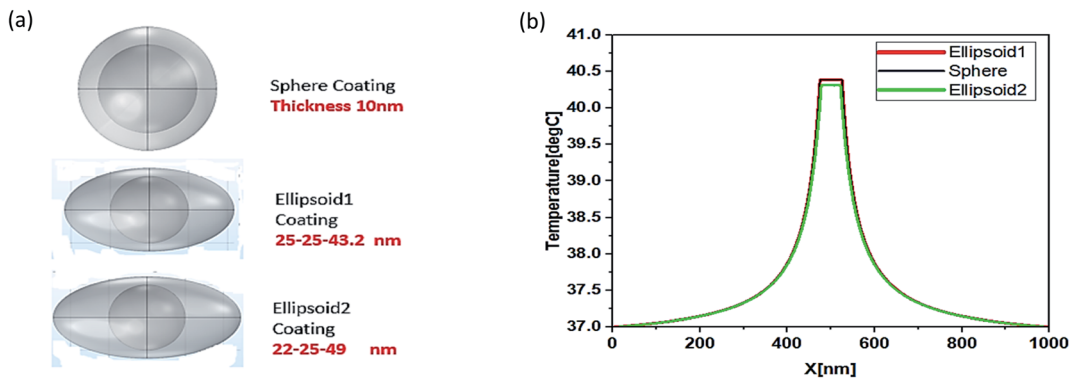

Fig. 6 (a) Different coating surfaces (b) the radial temperature distribution for various form of surface coating, Au nanosphere 20 nm in radius, Au $\mathrm{nanoellipsoid}_1$: 25-25-43.2 nm, Au nanoellipsoide: 22-25-49 nm.

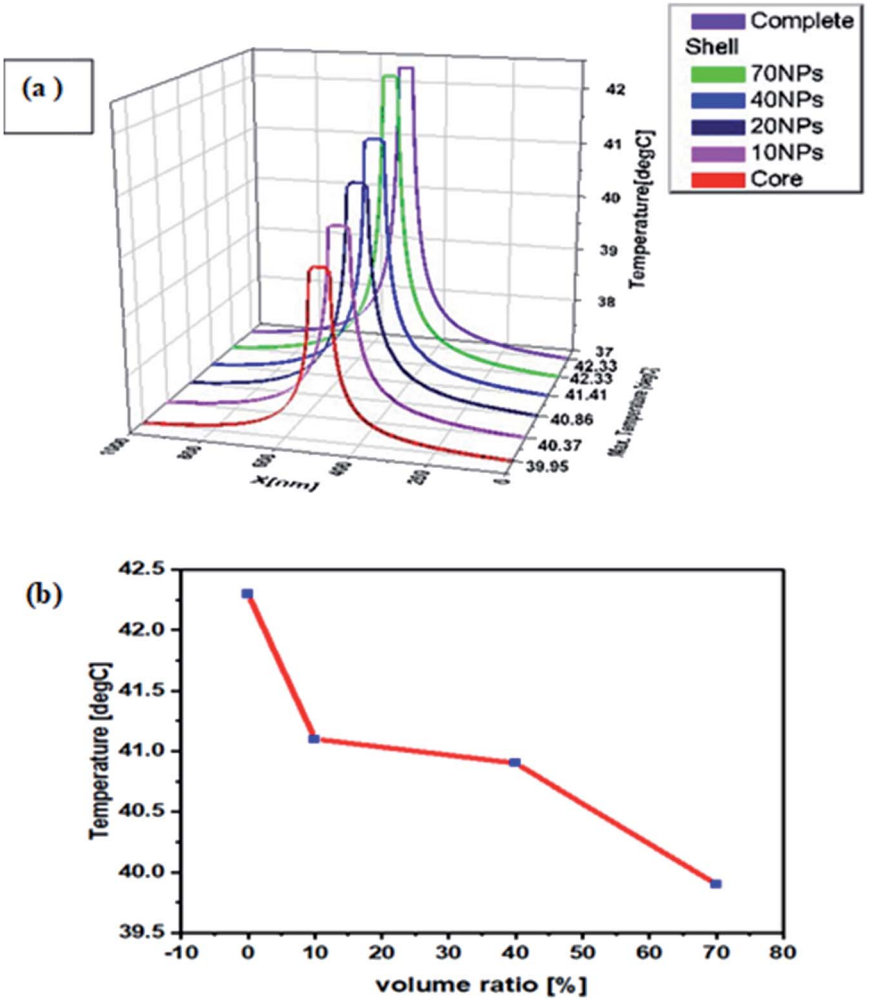

Fig. 7 (a) After 3 μs from the beginning of the heat process, the radial temperature distribution for varying amounts of surface coating. (b) Volume coverage ratio of gold NPs.

calculated. It was shown that the maximum temperature at the center of the NP was 42.3 °C for uncovered core, while the temperature gradually decreased as the amount of surface coating increased, and the minimum temperature was 39.95 °C at the center of the NP when complete shell designed.

4. Conclusions

In our simulation gold nanoparticles were used because of their antibacterial, antifungal, and antiviral properties. By using COMSOL Multiphysics, simulations were performed for 3 μs by using different shapes of gold nanoparticles like nanorod, nanosphere, and nano ellipsoid which were placed inside the spherical tumor tissue. It was found that the maximum temperature achieved by gold nanorod is higher than other shapes. Because the same volume and absorption speed particle was utilized, thermal equilibrium was established for all three simulated forms at the same time of 1 μs after the heating process began. The uniformity of the thickness and shape of the shell are examined, and the temporal characterization of the surface coating material/thickness ratio characterized the shell's thermal properties as a function of temperature change (increase/decrease). There is inverse relation between silver and PEG polymer coating materials *i.e.*, temperature increases with increase in coating surface of PEG polymer and decrease for silver coating. The shape of coating surface is anisotropy. The uniform thickness of the shell permits a little fluctuation in the maximum temperature of the core (less 0.5 °C). The heat response of various silver covering volume ratios is simulated, and the impact of partial surface coating is examined. It is observed that the open surface left by the growing process has a substantial impact on the temperature profile's development. Volume coverage ratio by small AgNPs reflex that temperature decreases with increasing volume coverage. The application of nanoparticles with a core and a functional biocompatible surface shell is based on material selection and surface homogeneity. This study suggests that gold nanoparticles with different shapes are good candidate for hyperthermia.

Data availability

Data will be generated after request.

Conflicts of interest

The authors declare no conflict of interest.

References

1 M. Singh, Doctoral dissertation, Thapar Institute of Engineering and Technology University, 2016.
2 S. K. Sharma, N. Shrivastava, F. Rossi and N. T. K. Thanh, *Nano Today*, 2019, **29**, 100795.
3 M. K. Shahzad, Y. Zhang, A. Raza, M. Ikram, K. Qi, M. U. Khan, M. J. Aslam and A. Alhazaa, *Nanoscale Res. Lett.*, 2019, **14**(270), 1–11.
4 G. Baronzio, G. Parmar, M. Ballerini, A. Szasz, M. Baronzio and V. Cassutti, *J. Integr. Oncol.*, 2014, **3**(115), 2–10.
5 P. Wust, B. Hildebrandt, G. Sreenivasa, B. Rau, J. Gellermann, H. Riess and P. M. Schlag, *Lancet Oncol.*, 2002, **3**(8), 487–497.
6 R. W. Habash, R. Bansal, D. Krewski and H. T. Alhafid, *Crit. Rev. Biomed. Eng.*, 2006, **34**(6), 491–542.
7 Z. Behrouzkia, Z. Joveini, B. Keshavarzi, N. Eyvazzadeh and R. Z. Aghdam, *Oman Med. J.*, 2016, **31**(2), 89–97.
8 S. K. Sharma, N. Shrivastava, F. Rossi and N. T. K. Thanh, *Nano Today*, 2019, **29**, 100795–100820.
9 M. K. Shahzad, Y. Zhang, M. U. Khan, H. Sattar and M. Ikram, *Curr. Appl. Phys.*, 2019, **19**, 739–744.
10 A. Farzin, S. A. Etesami, J. Quint, A. Memic and A. Tamayol, *Adv. Healthcare Mater.*, 2020, **9**(9), 1901058–1901064.
11 P. H. Wu, A. E. Opadele, Y. Onodera and J. M. Nam, *Cancers*, 2019, **11**(11), 1783–1790.
12 S. Kim, S. P. Surendran and Y. Y. Jeong, *Pharmaceutics*, 2019, **11**(7), 306–310.
13 E. C. Dreaden, A. M. Alkilany, X. Huang, C. J. Murphy and M. A. El-Sayed, *Chem. Soc. Rev.*, 2012, **41**(7), 2740–2779.
14 A. Ghulam, M. Afzaal, F. D. Nunes, M. Y. Naz, N. M. AbdEl-Salam, K. A. Ibrahim and Y. Khan, *AIP Adv.*, 2021, **11**(4), 045301–045310.
15 F. F. An and X. H. Zhang, *Theranostics*, 2017, **7**(15), 3667–3673.
16 R. R. Nasaruddin, T. Chen, N. Yan and J. Xie, *Coord. Chem. Rev.*, 2018, **368**, 60–79.
17 Y. Sun, W. Ma, Y. Yang, M. He, A. Li, L. Bai and Z. Yu, *Asian J. Pharm. Sci.*, 2019, **14**(6), 581–594.
18 M. J. Mitchell, M. M. Billingsley, R. M. Haley, M. E. Wechsler, N. A. Peppas and R. Langer, *Nat. Rev. Drug Discovery*, 2021, **20**(2), 101–124.
19 M. Najafi, B. Farhood and K. Mortezaee, *J. Cell. Physiol.*, 2019, **234**(6), 7983–7993.
20 Z. Wang, T. Jia, Q. Sun, Y. Kuang, B. Liu, M. Xu and P. Yang, *Biomaterials*, 2020, **228**, 119569.
21 R. Prasad, V. Kumar and K. S. Prasad, *Afr. J. Biotechnol.*, 2014, **13**(6), 705–713.
22 A. A. Abdellatif and H. M. Tawfeek, *Drug Dev. Ind. Pharm.*, 2018, **44**(10), 1679–1684.
23 X. Y. Wong, A. Sena-Torralba, R. Alvarez-Diduk, K. Muthoosamy and A. Merkoci, *ACS Nano*, 2020, **14**(3), 2585–2627.
24 M. A. Ibrahim and A. A. Abdellatif, *Nano pharmaceuticals: Principles and Applications*, 2021, vol. 1, pp. 73–114.
25 Y. Bai, T. Shu, L. Su and X. Zhang, *Crystals*, 2020, **10**(5), 357–364.
26 J. Yang, C. Wang, S. Shi and C. Dong, *Nano Res.*, 2020, **12**, 1–22.
27 R. Prasad, N. K. Jain, J. Conde and R. Srivastava, *Mater. Today Adv.*, 2020, **8**, 100087.
28 M. Back, T. C. Gasser, J. B. Michel and G. Caligiuri, *Cardiovasc. Res.*, 2013, **99**(2), 232–241.
29 R. Mittal, J. H. Seo, V. Vedula, Y. J. Choi, H. Liu, H. H. Huang and R. T. George, *J. Comput. Phys.*, 2016, **305**, 1065–1082.
30 C. Menichini and X. Y. Xu, *J. Math. Biol.*, 2016, **73**(5), 1205–1226.
31 S. Taloub, F. Hobar, I. Astefanoaei, I. Dumitru and O. F. Caltun, *Nanosci. Nanotechnol.*, 2016, **6**(1A), 55–61.
32 A. K. Rengan, A. B. Bukhari, A. Pradhan, R. Malhotra, R. Banerjee, R. Srivastava and A. De, *Nano Lett.*, 2015, **15**(2), 842–848.
33 M. Salloum, R. H. Ma, D. Weeks and L. Zhu, *Int. J. Hyperth.*, 2008, **24**(4), 337–345.
34 M. Johannsen, B. Thiesen, P. Wust and A. Jordan, *Int. J. Hyperth.*, 2010, **26**(8), 790–795.
35 C. T. Lin and K. C. Liu, *Int. Commun. Heat Mass Transfer*, 2009, **36**(3), 241–244.
36 M. Singh, Doctoral dissertation, Thapar Institute of Engineering and Technology University, 2016.
37 S. Malekie and A. Rajabi, *Int. J. Nanosci. Nanotechnol.*, 2020, **16**(3), 181–188.
38 M. K. Shahzad, Z. Yundong, L. Cui, L. Liu, M. K. Butt and H. Li, *RSC Adv.*, 2018, **8**, 19362–19368.
39 C. B. Saw, A. Loper, K. Komanduri, T. Combine, S. Huq and C. Scicutella, *Med. Dosim.*, 2005, **30**(3), 145–148.
40 A. O. Govorov, W. Zhang, T. Skeini, H. Richardson, J. Lee and N. A. Kotov, *Nanoscale Res. Lett.*, 2006, **1**(1), 84–90.
41 S. Tippa, M. Narahari and R. Pendyala, *AIP Conf. Proc.*, 2016, **1787**(1), 020014–020020.
42 D. H. Kim, D. E. Nikles and C. S. Brazel, *Materials*, 2010, **3**(7), 4051–4054.